RESEARCH ARTICLE-CHEMISTRY

Preparation and Characterization of Amoxicillin-Loaded Polyvinyl Alcohol/Sodium Alginate Nanofibrous Mat: Drug Release Properties, Antibacterial Activity, and Cytotoxicity

Azize Çerçi[1] · Elif Sena Demir[2] · Esra Karaca[3] · Çağla Bozkurt Güzel[2] · Bilgen Osman[4]

Abstract

This study aimed to prepare a polyvinyl alcohol/sodium alginate (PVSA) nanofibrous mat as an amoxicillin (AMOX) delivery system. AMOX was loaded to the PVSA nanofibers during electrospinning, and the AMOX-loaded PVSA (PVSA/AMOX) nanofibrous mat was cross-linked by glutaraldehyde (GA). The PVSA/AMOX nanofibrous mat was characterized by Fourier Transform infrared spectroscopy, scanning electron microscopy, Brunauer–Emmett–Teller, and mercury porosimetry analyses. The thickness, air permeability, and water vapor transmission rate of the PVSA/AMOX nanofibrous mat were 0.43 ± 0.08 mm, 17.2 ± 4.91 L/m^2/s, and 1485 ± 13.6 g/m^2/d, respectively, which were suitable for wound dressing applications. The tensile strength was 6.73 ± 0.48 MPa and elongation at a maximum load was $81.9 \pm 17.0\%$, within the ranges of human skin's values. The total porosity was 59.4%, enabling cell adhesion, migration, and proliferation. The PVSA/AMOX nanofibrous mat has high swelling ($319 \pm 4.2\%$) and low degradation ($2.2 \pm 0.1\%$ in 10 days) ratios. The nanofibrous mat cross-linked with 0.25% GA solution for 20 min had a 73.07% cumulative release for 90 min. The drug release kinetics were obeyed to the Korsmeyer-Peppas model. The nanofibrous mat presented antibacterial activity on *S. aureus* ATCC 29213 and *E. coli* ATCC 25922, and there was no cytotoxic effect on the human normal keratinocyte cells, demonstrating the potential for use in wound dressing applications.

Keywords Drug release · Amoxicillin · Electrospinning · Antibacterial activity · Wound dressing

✉ Bilgen Osman
   bilgeno@uludag.edu.tr

   Azize Çerçi
   azizecrc@gmail.com

   Elif Sena Demir
   elifsenademir@gmail.com

   Esra Karaca
   ekaraca@uludag.edu.tr

   Çağla Bozkurt Güzel
   cagla.bozkurt@istanbul.edu.tr

1 Department of Biomaterials, Graduate School of Natural and Applied Sciences, Bursa Uludag University, 16059 Gorukle, Bursa, Turkey

2 Department of Pharmaceutical Microbiology, Faculty of Pharmacy, Istanbul University, 34116 Fatih, Istanbul, Turkey

3 Department of Textile Engineering, Faculty of Engineering, Bursa Uludag University, 16059 Gorukle, Bursa, Turkey

4 Department of Chemistry, Faculty of Arts and Science, Bursa Uludag University, 16059 Gorukle, Bursa, Turkey

1 Introduction

Wound dressings increase tissue regeneration directly or indirectly and promote wound healing. Medicated dressings, wound care products releasing anti-microbial agents, anti-inflammatory drugs or bioactive molecules, have been used to promote the healing process indirectly by removing necrotic tissue or directly by enhancing wound healing stages [1]. In the case of chronic wounds in which the patients are often subject to long treatments and frequent dressing changes, a system that delivers drugs to the wounded area improves therapeutic outcomes and patient compliance [2]. In this regard, bioadhesive polymeric dressings have great application potential, especially for treating local infections requiring high local antibiotic concentration. The drug-loaded wound dressings also provide great convenience due to their tissue compatibility, bacterial resistance, and reduced intervention in wound healing [3].

🍎 Springer

Nanofiber-based wound dressings prepared by electrospinning provide significant advantages in wound healing. Because the tissues mainly comprise hierarchical nanofibrous structures, electrospun scaffolds perfectly mimic the biological systems and attract fibroblast cells to the dermal layer, which is necessary for repairing damaged tissues [4]. Owing to their superior physical properties, the nanofibers absorb wound exudate ideally and provide a moist environment for cell respiration and proliferation. In addition, the nanofibers' tiny pores reduce the risk of bacterial invasion, provide high permeability, and protect injured tissue from dehydration [5].

The direct integration of the drugs into nanofibers is achieved via electrospinning of the polymer solution, including drugs or adsorption of drugs onto/within the nanofibers [6]. Since wound infection is a serious problem that can induce severe complications, nanofibrous wound dressings are generally loaded with antibacterial agents such as silver nanoparticles [7], small molecules [8], polymers [9], drugs [10] or growth factors [11] to achieve an optimum healing performance. Polyvinyl alcohol (PVA) and sodium alginate (SA) are polymers used widely for wound dressing applications. PVA, a biocompatible and non-toxic synthetic polymer, has attracted considerable attention in biomedical applications due to its chemical and thermal stability and water absorption capacity [12]. SA is a polysaccharide derived from brown algae. It has hemostatic properties. SA can absorb exudate and promote hemostasis in wound healing owing to its super absorbency [13]. SA has been widely used in wound dressing applications, and there are many commercially available alginate-based wound dressings. Due to its polyelectrolyte characteristics and inadequate chain entanglement, SA cannot be used for electrospinning. Therefore, synthetic polymers such as PVA and polyethylene oxide have been added to aqueous SA solutions in electrospinning [14]. A limited number of studies have been reported for PVA/alginate-blended electrospun nanofibers [14–17]. SA and PVA blend improves the final wound-healing material's physical, mechanical, and biological properties compared to the individual polymers. Therefore, biomaterials, including PVA/SA, are promising for wound treatment [18]. Various drugs have been loaded into PVA/SA nanofibers to improve wound healing performance. In this regard, the preparation of PVA/SA nanofibers loaded with different drugs and natural products such as ciprofloxacin [10], purple cabbage (Brassica oleracea) anthocyanins [19], ZnO nanoparticles [20], organic rectorite [21], essential oils [22], moxifloxacin hydrochloride [23], naftifine [24], nano-curcumin/graphene platelets [25], lutein [26], gatifloxacin hydrochloride [27] and cardamom extract [28] have been reported for wound dressing applications.

Amoxicillin (AMOX), which is one of the essential antibiotics of the penicillin family with a broad bactericidal effect, antimicrobial activity, and a high therapeutic index, has recently attracted a great deal of attention because it is in the essential drug list of the World Health Organization. The American Food and Drug Administration approves its usage in drug delivery systems. Nanofibers such as cellulose acetate (CA)/polyvinyl pyrrolidone (PVP) [29, 30], CA/gelatin [31], gellan/PVA [32], poly (acrylamide-*co*-acrylic acid) [33], poly (lactide *co*-glycolic acid (PLGA)/hydroxyapatite/collagen [34], PLGA/collagen [35], sodium montmorillonite/poly (ester-urethane) urea [36], PLGA [37], Bombyx mori silk fibroin/PVA [38] and chitosan [39] were used as AMOX carriers for controlled drug release applications. To the best of our knowledge, no research has been done to exploit the superior characteristics of PVA/SA nanofibers as a wound dressing for the delivery of AMOX until now.

This study mainly aims to prepare a polyvinyl alcohol/sodium alginate (PVSA) nanofibrous mat via electrospinning as an AMOX delivery system. The cross-linked AMOX-loaded PVSA (PVSA/AMOX) nanofibrous mat was prepared by glutaraldehyde (GA). The characterization studies were conducted by Fourier transform infrared spectroscopy (FTIR), scanning electron microscopy (SEM), Brunauer–Emmett–Teller (BET), and mercury porosimetry analyses. In addition, swelling and hydrolytic degradation properties, water contact angle (WCA) and thickness, water vapor transmission rate (WVTR), air permeability, and tensile strength of the nanofibrous mat were determined. The effect of GA amount and cross-linking time on drug release profiles of the PVSA/AMOX nanofibrous mat was investigated in detail. The release kinetic models were applied to cumulative release data. The antibacterial activity of the PVSA/AMOX nanofibrous mat was investigated by disc diffusion assay and bacterial colony counting assay on Grampositive bacteria (*S. aureus* ATCC 29213) and Gram-negative bacteria (*E. coli* ATCC 25922). Cytotoxicity studies were conducted using human normal keratinocyte cells (HaCaT).

2 Experimental

2.1 Materials

Amoxicillin trihydrate ($C_{16}H_{19}N_3O_5S.3H_2O$; MW:419.45 g mol^{-1}) was obtained from Alfa Aesar (J61290). SA (viscosity range: 700–900 cP) was purchased from Cargill (Cecalgum® S1300). PVA (MW: 85.000–124.000 g mol^{-1} and 87–89% hydrolyzed) for electrospinning was obtained from Sigma-Aldrich. Tryptic Soy Agar (TSA), Mueller Hinton Agar (MHA), and Tryptic Soy Broth (TSB) mediums used to perform antibacterial tests

were prepared according to the manufacturer's instructions. HaCaT cells were cultured in Dulbecco's Modified Eagle's Medium (DMEM-F12) (Sigma-Aldrich) supplemented with 10% fetal bovine serum (FBS; Sigma-Aldrich) and 1% penicillin/streptomisin (Sigma-Aldrich).

2.2 Preparation of the PVSA/AMOX Nanofibrous Mat

PVSA electrospinning solution was prepared by mixing 12% (w/v) PVA and 1% (w/v) SA solutions at a ratio of 2/1 (v/v). For this purpose, a 12% PVA (w/v) solution was first prepared by mixing PVA in pure water at 90 °C for 6 h. For 1% (w/v) SA solution, SA was mixed in purified water for 6 h at 60 °C. Both solutions were kept at room temperature for 24 h. Then, the PVSA solution, prepared by mixing 12% PVA and 1% SA solutions at a ratio of 2/1 (v/v), was mixed at room temperature for 4 h until it became homogeneous. PVSA/AMOX electrospinning solution was prepared by adding 6.4 mg amoxicillin trihydrate to the PVSA solution (20 mL). Viscosity (Brookfield RV-DV II Viscometer), surface tension (KSV contact angle and surface tension meter), electrical conductivity (HANNA HI-98129 conductivity meter), and pH (HANNA HI2020-02 Edge Digital pH-meter) of the PVA, SA, PVSA, PVSA/AMOX solutions were determined. All measurements were carried out at 25 °C.

The nanofibrous mats (PVSA and PVSA/AMOX) were constructed using the Inovenso brand (Starter Kit, Turkey) electrospinning device. The solution feed rate and distance between the nozzle and collector roller were 0.5 mL/h and 15 cm, respectively. The applied voltage was 25 kV. A syringe with a 21-gauge needle was used as the feeding unit. The nanofibers were collected on aluminum foil wrapped around a cylindrical drum rotating at 200 rpm.

GA cross-linking was applied to increase the stability of the nanofibrous mats to hydrolytic degradation. In a typical cross-linking procedure, the nanofibrous mats (2 cm × 2 cm) were immersed in an acetone solution, including HCl and GA, at room temperature. After that, they were washed with acetone, ethyl alcohol, and PBS (pH 7.4) and dried at room temperature for 24 h. To evaluate the effect of cross-linker amount and cross-linking time on the AMOX release profile, the nanofibers were cross-linked by using GA solutions at a concentration of 0.25% (v:v), 0.5% (v;v) and 1% (v:v) GA for 20 min and 40 min.

2.3 Characterization Studies

FTIR analyses of the nanofibrous mats were performed in the 400–4000 cm^{-1} frequency range. Analysis was performed using an FTIR spectrophotometer (Perkin Elmer Spectrum 100 Waltham, MA, USA) with ATR apparatus.

The morphological visualization was achieved by a scanning electron microscope (Carl Zeiss AG-EVO 40 XVP).

Image J software (National Institute of Health, USA) was used to determine mean nanofiber diameter and diameter distribution via 100 random measurements.

The nanofibrous mat's specific surface area, pore size, and pore volumes were determined through a BET isotherm of nitrogen with an ASAP2000 instrument (Micromeritics). The porosity of the nanofibrous mat was determined in terms of mercury porosimetry (Quantachrome Corporation, Poremaster 60). The applied pressure was 30,000 psi.

The hydrophilicity of the nanofibrous mats was investigated via WCA measurements using the sessile drop method by Attention Theta contact angle instrument. The WCAs were measured by taking 40 separate photos of the different parts of the surface.

The swelling ratio (%) of the nanofibrous mats in PBS (pH 7.4) at 25 °C was determined at different time intervals [40]. Briefly, the dried nanofibrous mats were weighed and then immersed in PBS solution. The swelled samples taken at specific intervals were weighed after wiping with filter paper. The swelling ratio (%) was calculated according to Eq. (1);

$$Swelling\,ratio(\%) = \left(\frac{Ws - Wd}{Wd} \right) \times 100 \qquad (1)$$

where W_s is the weight of swollen nanofibers, and W_d is the weight of dried mats.

Hydrolytic degradation studies were conducted by measuring the remaining mass [41]. Briefly, dry nanofibrous mats (2 cm × 2 cm) were weighted and immersed in PBS. The nanofibrous mats were drip-dried with filter paper at different times and placed in an oven at 30 °C for 3 days. The degradation ratio (%) was calculated using Eq. (2);

$$Degradation\,ratio(\%) = \left(\frac{Wo - Wt}{Wo} \right) \times 100 \qquad (2)$$

where W_o is the initial weight of dry nanofiber and W_t is the weight of dried samples after the degradation.

A digital micrometer was used to measure the thickness of the nanofibrous mats (INSIZE Thickness Gauge). The measurements were made with a 0.005 mm accuracy at five points. The tests were conducted at 25 ± 2 °C.

The tensile test was carried out using the Shimadzu AG–X plus brand tensile testing device. The nanofibrous mat with a dimension of 5 mm × 50 mm placed between the jaws of the test device was pulled until it broke using a 50 N load cell with a distance of 25 mm between the jaws and a jaw speed of 15 mm/min (ASTM D 3822 standard). The test obtained values of maximum load and extension at maximum load. The experiments were repeated five times, and the mean and standard deviations (SD) were calculated.

The air permeability test for the nanofibrous mat was applied by the SDL ATLAS M021A Air Permeability Tester.

The test was performed in 5 cm^2 under 98 Pa pressure according to the BS 5636 standard. The measurements were repeated three times, and the mean and SD were calculated.

The WVTR test was applied using the E96-00 standard method at 37 °C and 85% relative humidity (ASTM E 96-95, Annual Book of ASTM, 1995). The nanofibrous mat was cut into a circle, placed in the mouth of a 13.6 mm diameter glass bottle containing 10 mL of pure water, and weighed. Then, the bottle was kept in a desiccator containing saturated ammonium sulfate solution at 37 °C for 24 h. The bottle was weighed again after 24 h. Experiments were repeated three times. The WVTR value (g/m^2/day) was calculated using Eq. (3) [42].

$$WVTR = (W_o - W_f)/10^6 A \qquad (3)$$

where A is the area of the mouth of the bottle (mm^2); W_o and W_f are the weight (g) of the bottle before and after 24 h of storage at 37 °C, respectively.

2.4 In Vitro Drug Release

The in vitro drug release studies were performed in a beaker using PBS (pH 7.4, 2 mL) as a release medium at 37 °C under stirring in a shaking incubator at 50 rpm. The release medium was replaced with fresh medium at determined time intervals. The cumulative release (%) of the AMOX was calculated using Eq. (4);

$$Cumulative release(\%) = \left(\frac{W_t}{W_c}\right) \times 100 \qquad (4)$$

where W_c is the total amount of drug loaded onto the nanofibrous mat and W_t is the total amount of drug released in the release medium at time t.

The AMOX release was followed by a UV spectrophotometer (Shimadzu UV-1700). The calibration curve was prepared in the AMOX concentration range of 1–50 mg/L at a wavelength of 227 nm. The amount of loaded AMOX (mg AMOX/g nanofibrous mat) was calculated by dissolving three PVSA/AMOX nanofibrous mats in PBS solutions and determining the AMOX concentration. The amount of AMOX loaded into the nanofibrous mat was determined as 3.98 ± 0.04 mg/g nanofibers.

2.5 In Vitro Antibacterial Activity Studies

2.5.1 Preparation of Test Bacteria

The antibacterial activity of the PVSA/AMOX nanofibrous mat was investigated against *S. aureus* ATCC 29213 and *E. coli* ATCC 25922 via disc diffusion assay and bacterial colony counting assay. Overnight test cultures were prepared

in TSB and incubated at 37 °C for 24 h. The strains were adjusted to 0.5 McFarland turbidity standards with sterile media. Subsequently, the bacterial suspension was diluted to 1×10^6 CFU/mL to obtain an equal final bacteria load for disc diffusion assay and bacterial colony counting assay.

2.5.2 Bacterial Colony Counting Assay

The colony counting method was carried out as described earlier by Ozcan et al. 2023 [43]. Each surface of the PVSA/AMOX nanofibrous mats was sterilized by UV for 30 min. 85 mg of the nanofibrous mats were exposed to test bacteria suspension (1×10^6 CFU/mL) in 20 mL tubes incubated at 37 °C for 2 h, 4 h, 6 h, and 24 h. At various exposure times, 1 mL bacterial suspension was taken and diluted between 10^1 to 10^9 in 9 mL saline solution. Then, 0.1 mL of the diluted bacterial suspension was spread onto a TSA plate and incubated at 37 °C for 24 h. The colonies were counted, and nanofibrous mats' bacterial inhibition (%) was calculated using Eq. (5).

$$\begin{aligned} Bacterial inhibition\,(\%) \\ = (log\,PVSA - log\,PVSA/AMOX)\,/log\,PVSA\,x\,100 \end{aligned} \qquad (5)$$

2.5.3 Disc Diffusion Assay

For the disc diffusion assay, the inoculum (1×10^6 CFU/mL) was spread onto MHA, and the nanofibrous mats cut into the diameter of 1 cm were placed on the center of the medium. The Petri dishes were incubated at 37 °C for 24 h, and the inhibition zone diameter was measured by a digital caliper [44].

2.5.4 Statistical Analysis

Data were given as mean $\pm$ SD. Statistical analyses were performed using SPSS version 22 (IBM, New York, USA) at a 95% confidence interval. The control and PVSA/AMOX nanofibrous mat results of each bacteria and log reduction at the same time interval were evaluated with the independent sample t-test. Log reduction data at the different time intervals for each bacterium were analyzed with one-way ANOVA, and the differences were compared with Duncan's multiple-range test.

2.6 Cytotoxicity Studies

To best mimic the intended use of nanofibrous mats, HaCaT cells were used in cytotoxicity studies. Cell viability was determined by MTT (3-(4,5-dimethylthiazol-2-yl)-2,5-diphenyltetrazolium bromide) cell viability method [45, 46].

Amoxicillin trihydrate stock solution was prepared with dimethyl sulfoxide (DMSO) (final DMSO concentration of 0.1% in cell culture) and filtered with 0.22 μm PES membrane filter. Nanofibrous mats (PVSA and PVSA/AMOX) were first cross-linked with GA solution at 0.25% concentration for 20 min. Sections of 0.32 mm radius (0.32 mm^2) were taken from the nanofibrous mats, and each well of the 96-well cell culture dish was coated. Ultra-low attachment plates were used to prevent cells from adhering to the surface of the cell culture plate other than the nanofibrous mat. They were then sterilized with UV light for 12 h and used in cytotoxicity studies.

HaCaT cells were maintained at 37 °C and 5% CO_2 using DMEM-F12 containing 10% FBS, 2 mM L-glutamine and 100 U/mL penicillin–streptomycin. After 80% confluence, the cells were seeded in a 96-well cell culture plate with nanofibrous mats at a rate of 5×10^3 cells per well. After 48 and 72 h of incubation, 20 μL MTT was added to all wells. After 4 h, 100 μl of dissolution solution (0.2% NP-40 and 4 mM HCl) was added to dissolve the formazan crystals. Optical density values were measured at 570 nm wavelength using a BioTek multimode microplate reader. For each sample, the mean and SD obtained from six wells were determined and given as cell viability (%) relative to control.

3 Results and Discussion

3.1 Morphological and Chemical Characterization of the Nanofibrous Mats

In the electrospinning method, producing nanofibers with desired properties strongly depends on the solution parameters. Therefore, the solution parameters (viscosity, pH, conductivity, and surface tension) for PVA (12%, w/v), SA (1%, w/v), PVSA (2/1, v/v), and PVSA/AMOX (2/1, v/v) solutions were determined and summarized in Table 1. It was clear that adding SA solution to PVA solution did not cause a significant change in the pH and surface tension; however, it caused a severe decrease in viscosity, probably because of the intermolecular interactions between the polymer chains. By the way, the SA solution with a high conductivity caused a significant increase in the conductivity of the PVSA solution due to the negatively charged COO^- groups of SA. The addition of AMOX into the PVSA solution caused insignificant changes in the viscosity, pH, and surface tension of the PVSA solution. On the other hand, the conductivity of the PVSA/AMOX solution was higher than that of the PVSA solution since AMOX has a net charge at the pH of the electrospinning solution.

The morphological analyses of the nanofibrous mats were conducted by SEM. The SEM images of the PVSA and the PVSA/AMOX nanofibrous mats are given in Fig. 1. The effect of drug integration on the nanofiber morphology was evaluated by determining the average nanofiber diameter and diameter distribution, which was calculated from SEM images. The images clearly showed that the PVSA and the PVSA/AMOX nanofibers were beadles, ultrafine, and uniform. The average diameter of the PVSA/AMOX nanofibers (201.7 ± 30.9 nm) was higher than that of PVSA nanofibers (171.9 ± 42.1 nm), demonstrating the integration of AMOX in the nanofibrous mat. Integration of drug molecules into the nanofibers generally increases the nanofiber diameter [47].

The PVSA and the PVSA/AMOX nanofibrous mats cross-linked at different GA concentrations (0.25%, 0.5%, and 1%) for 20 min cross-linking time were also visualized by SEM analyses. SEM images and average nanofiber diameters and diameter distributions are given in Fig. 2. It can be seen that the average diameters of the nanofibers increased after GA cross-linking due to the flattening of the nanofibers [19, 48, 49]. In addition, the fusions were observed at junction points of nanofibers, which were observed more clearly in the nanofibers (PVSA and PVSA/AMOX) cross-linked at 0.25% GA. Since the cross-linking time did not significantly affect the nanofiber morphology and the average nanofiber diameter, SEM images of the nanofibrous mats cross-linked for 40 min were not given. For 20 min, the average diameters of the cross-linked PVSA nanofibrous mat and the cross-linked PVSA/AMOX nanofibrous mat ranged between 206.1 ± 38.5 nm to 248.4 ± 75.6 nm and 201.9 ± 36 nm to 238.5 ± 45.3 nm, respectively. As a result, the mean nanofiber diameter of the PVSA and PVSA/AMOX nanofibrous mats did not significantly change after cross-linking. Moreover, there was no significant difference between the mean nanofiber diameters of the PVSA/AMOX and PVSA nanofibrous mats cross-linked at different GA concentrations.

The FTIR spectra of the PVSA, PVSA/AMOX, and cross-linked PVSA/AMOX nanofibrous mats are given in Figure SI1. The functional groups in the spectra are also summarized in Table 2. The absorption band of acetal bonds (C–O–C) observed at 1126 cm^{-1} in the FTIR spectrum of the cross-linked PVSA/AMOX nanofibers proved that the nanofibrous mat was successfully cross-linked with GA [48, 49]. The intensity of the adsorption band belonging to –OH groups decreased sharply after cross-linking with GA. The aldehyde group C–H stretching band observed at 2861 cm^{-1} in the spectrum of cross-linked PVSA/AMOX nanofibrous mat demonstrated the existence of unreacted aldehyde ends of GA molecules.

3.2 AMOX Release from the PVSA/AMOX Nanofibrous Mats

AMOX release studies were conducted for the PVSA/AMOX nanofibrous mats that were only cross-linked with GA solutions in the 0.25% and 1% concentrations at cross-linking

Table 1 Solution parameters

Solution	Viscosity (cp)	pH	Surface Tension (N/m)	Conductivity (µS/cm)
PVA	1069	5.67	56.90	384
SA	32	6.44	84.37	1785
PVSA	230.4	5.40	58.88	1188
PVSA/AMOX	182.4	5.33	41.76	1478
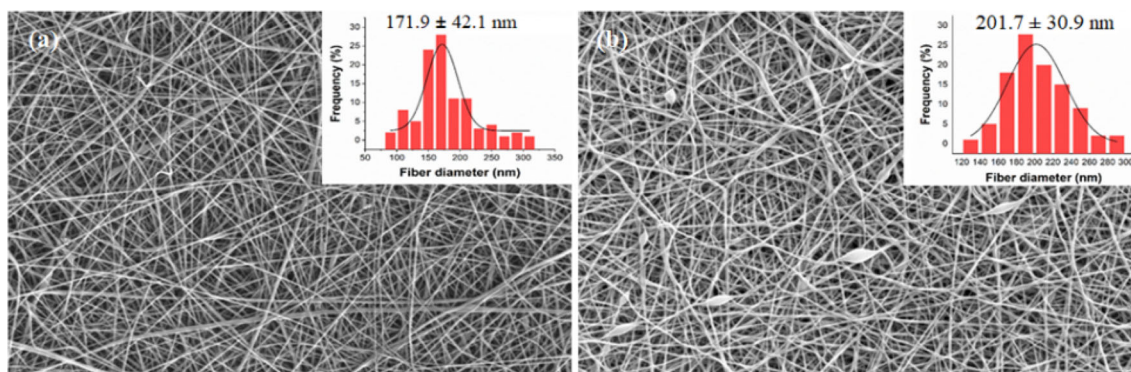
Fig. 1 SEM images, average nanofiber diameters and diameter distributions of the **a** PVSA and **b** PVSA/AMOX nanofibrous mats
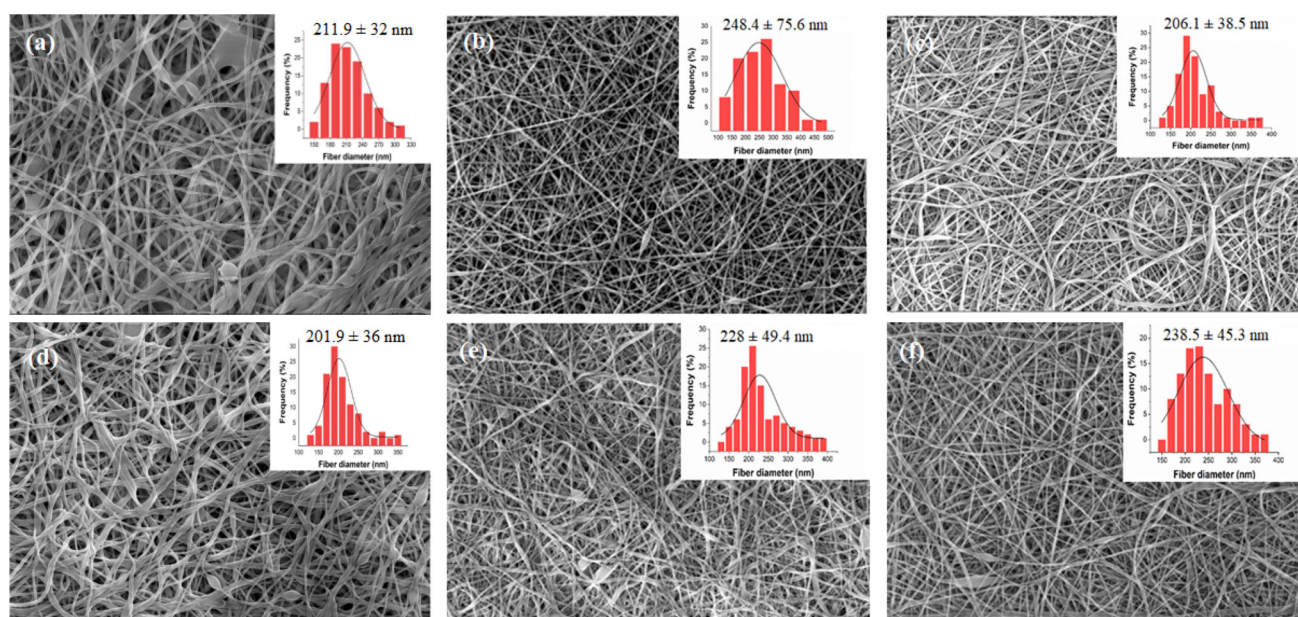
Fig. 2 SEM images, mean nanofiber diameters and diameter distributions of the cross-linked PVSA nanofibrous mats (**a**, **b**, **c**) and the cross-linked PVSA/AMOX nanofibrous mats **d**, **e**, **f** prepared at 0.25% GA, 0.5% GA and 1% GA concentrations (cross-linking time: 20 min), respectively

times of 20 min and 40 min (Fig. 3). The cumulative release (%) data for the PVSA/AMOX nanofibrous mat cross-linked with GA solution in the 0.5% concentration at the same cross-linking times were not investigated since they had no antibacterial activity. The results in Fig. 3 showed that the concentration of GA solution significantly affected the release profile. The cumulative release (%) for the PVSA/AMOX nanofibrous mats cross-linked with 0.25% and 1% GA solutions for 20 min was 73.07% for 90 min

and 20% for 5 days, respectively. The AMOX release from the PVSA/AMOX nanofibrous mats cross-linked with 1% GA solution for 20 min and 40 min started after 1 day. The cumulative release (%) from PVSA/AMOX nanofibrous mat cross-linked with 1% GA decreased from 20 to 15% for 5 days, when the cross-linking time increased from 20 to 40 min. The results clearly showed that penetration of water molecules to the polymer chains drastically decreased

Table 2 The functional groups of the PVSA, PVSA/AMOX, and cross-linked PVSA/AMOX nanofibrous mats

Wavenumber (cm^{-1})			Identified groups
PVSA	PVSA/AMOX	Cross-linked PVSA/AMOX	
3315	3315	3391	– OH groups
2918	2918	2922	C–H (alkyl group)
–	–	2861	C–H (aldehyde)
1733	1733	1733	C=O (ester carbonyl)
1091	1091	–	C–O stretching
–	–	1126	C–O–C (acetal bond)

with the increasing cross-link density, preventing drug diffusion. Consequently, the PVSA/AMOX nanofibrous mat cross-linked at 1% GA solution was not suitable to use as a carrier for AMOX release. At a GA % concentration of 0.25, controlled AMOX release was observed for 90 min with a cumulative release of 73.07% and 55.71% for 20 min and 40 min cross-linking, respectively. The increase in the cross-linking time caused a decrease in the cumulative release (%). From a clinical point of view, an initial rapid release in the early stages is beneficial because it helps achieve a therapeutic concentration of the drug in minimal time, followed by sustained release to maintain a minimal effective concentration [50].

The drug release data obtained from the PVSA/AMOX nanofibers cross-linked by 0.25% GA solution for 20 min and 40 min were fitted to the kinetic models (the zero-order, the first-order, the Higuchi, and the Korsmeyer–Peppas).
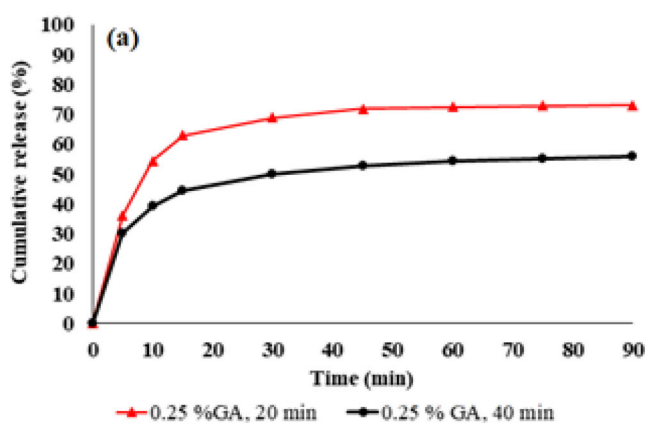
The equations of applied models and the values of constants obtained from the slopes and intercepts of the fitted curves are summarized in Table 3, Figure SI2, and Figure SI3. In the equations, Qt (%) is the amount of drug released in t time, Q_o (%) is the initial amount of drug in the solution, and $Q\infty$ (%) is the equilibrium amount of drug in the medium. K_o (min^{-1}), K_1 (min^{-1}), K_H (min$^{-1/2}$), and K_m (min^{-1}) are the zero-order model, the first-order model, the Higuchi kinetic model, and the Korsmeyer-Peppas model release constant, respectively. n is the release exponent of the Korsmeyer–Peppas model. The drug release followed the Korsmeyer–Peppas kinetic models with correlation coefficients (R^2) higher than 0.8710 for PVSA/AMOX nanofibrous mats prepared at 0.25% GA for 20 min and 40 min cross-linking time. The release exponent (n) was calculated as 0.29 and 0.25 for the PVSA/AMOX nanofibrous mats prepared at 0.25% GA for 20 min and 40 min, respectively. The Higuchi model explains the drug release regarding diffusion based on Fick's law [51]. The transport mechanism of release is determined by using the Korsmeyer–Peppas model, which defines drug release as diffusion of the drug and erosion of the polymer matrix. Since all release exponent n was lower than 0.5, the mechanism of drug release obeyed Quasi–Fickian diffusion, referring to the non-swellable matrix diffusion [52].

3.3 Antibacterial Activity

S. aureus and *E. coli* were selected to determine the PVSA/AMOX nanofibrous mats' antibacterial activity since both bacteria have caused various infections [53, 54]. Among the tested nanofibrous mats cross-linked with different GA concentrations (0.25%, 0.5%, and 1%), only the PVSA/AMOX nanofibrous mat cross-linked at 0.25% GA concentration for 20 min shown antimicrobial activity on test bacteria. The result might be attributed to the
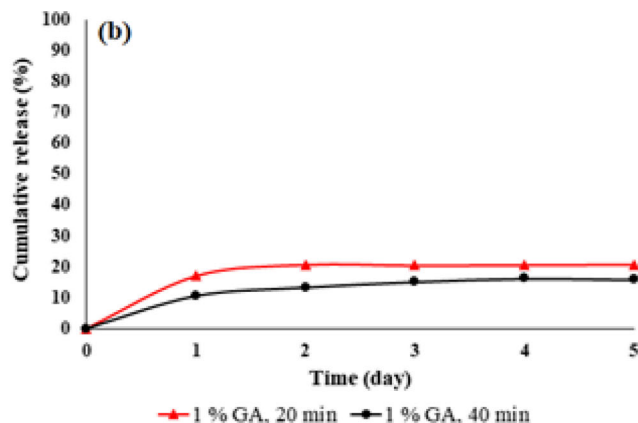
Fig. 3 The cumulative release (%)-time curves for the PVSA/AMOX nanofibrous mats cross-linked by **a** 0.25% GA and **b** 1% GA solutions for different cross-linking times

Table 3 Kinetic parameters of drug release from the cross-linked PVSA/AMOX nanofibrous mats

Models and parameters	Cross-linked PVSA/AMOX nanofibrous mats	
	(0.25% GA, 20 min)	(0.25% GA, 40 min)
Zero order $Q_t = Q_o + K_o t$		
Equation	y = 0.3162x + 50.998	y = 0.2514x + 37.329
R^2	0.5923	0.7485
$K_o (\text{min}^{-1})$	0.3162	0.2514
$Q_o (\%)$	50.99	37.33
Q_e	73.07	55.71
First order $\log Q_t = \log Q_o + \frac{K_1 t}{2.303}$		
Equation	y = 0.0024x + 1.6967	y = 0.0025x + 1.5687
R^2	0.5234	0.6823
$K_1 (\text{min}^{-1})$	5.52×10^{-3}	5.75×10^{-3}
$Q_o (\%)$	49.74	37.04
Q_e	73.07	55.71
Higuchi $Q_t = K_H \cdot t^{1/2}$		
Equation	y = 4.161x + 39.413	y = 3.2082x + 28.709
R^2	0.7304	0.8682
$K_H (\text{min}^{-1/2})$	4.161	3.2082
Korsmeyer–Peppas $\log \frac{Q_t}{Q_\infty} = \log K_m + n \log t$		
Equation	y = 0.1908x + 1.5138	y = 0.2508x + 1.3266
R^2	0.8710	0.9511
$K_m (\text{min}^{-1})$	25.23	21.21
n	0.29	0.25

Table 4 The log values for the cross-linked PVSA and PVSA/AMOX nanofibrous mats

| Bacteria	Nanofibrous mats	Time (h)				
		0	2	4	6	24
S. aureus (ATCC 29213)	PVSA (Control)	5.45 ± 0.015[a]	5.23 ± 0.040[a]	6.52 ± 0,010[a]	6.73 ± 0.025[a]	9.47 ± 0.045[a]
	PVSA/AMOX	5.25 ± 0.035[b]	5.22 ± 0.020[a]	4.74 ± 0,025[b]	4.44 ± 0.030[b]	5.22 ± 0.020[b]
	Log reduction	0.21 ± 0.04[aD]	0.01 ± 0.050[aE]	1.78 ± 0.01[aC]	2.29 ± 0.00[aB]	4.25 ± 0.05[aA]
E. coli (ATCC 25922)	PVSA(Control)	5.52 ± 0.015[a]	5.77 ± 0.020[a]	6.13 ± 0.025[a]	6.41 ± 0.020[a]	8.96 ± 0.030[a]
	PVSA/AMOX	5.44 ± 0.010[b]	5.76 ± 0.006[a]	5.10 ± 0.015[b]	5.05 ± 0.035[b]	6.25 ± 0.020[b]
	Log reduction	0.08 ± 0.01[bD]	0.01 ± 0.02[aD]	1.03 ± 0.01[bC]	1.36 ± 0.03[bB]	2.71 ± 0.04[bA]

Data were expressed as mean ± SD (n = 3)

[a−b]Different lower case letters in superscript within a column (at same time) for each bacterium indicate significant differences ($p < 0.05$) between PVSA (control) and PVSA/AMOX

[A−E]Different uppercase letters in superscript within a line for each bacterium indicate significant differences ($p < 0.05$) between the time and log reduction

[a−b]Additionally, different lower case letters in superscript within log reduction lines for the same time period indicate significant differences ($p < 0.05$) between log reduction and bacteria

Fig. 4 Bacterial inhibitions (%) at different time intervals for the cross-linked PVSA/AMOX nanofibrous mat

	2h	4h	6h	24h
■ E.coli	0.17	16.8	21.21	30.25
⋈ S.aureus	0.19	27.3	34.02	44.87
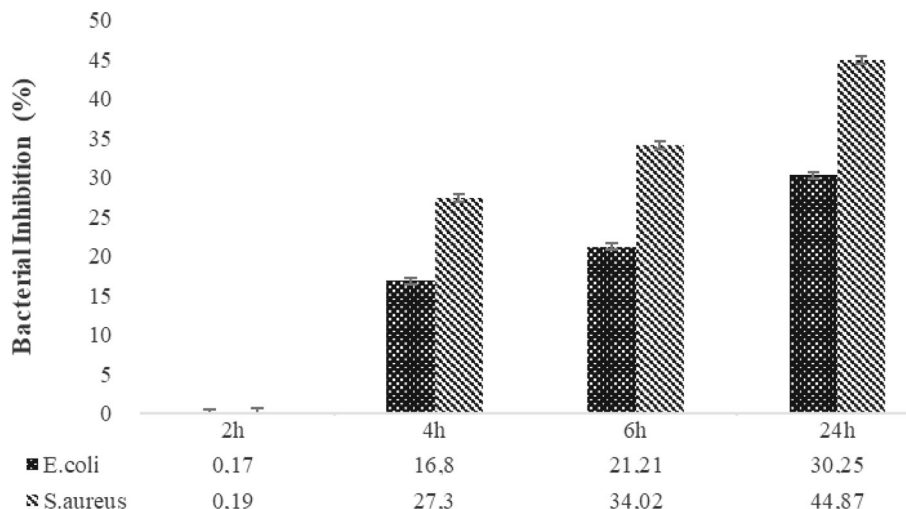
drug release kinetics from the polymeric materials because the drug release kinetics from the polymeric materials are affected by the chemical nature of the drug/polymer and cross-link density. The cross-link density of the polymer in which the drug was loaded is as essential as the hydrophilicity/hydrophobicity of the polymer. Linking polymer chains through chemical linkages gives a material a more rigid structure. The swelling of polymers decreases with increased cross-linking ratio due to tighter structures. Moreover, the drug may not diffuse into the medium at high cross-link density. The result matches the drug release kinetics observed for 0.25% and 1% GA cross-linking. Additionally, the PVSA/AMOX nanofibrous mat cross-linked at 0.25% GA concentration for 20 min presented a higher cumulative release (%) ratio than the nanofibrous mat cross-linked for 40 min. The PVSA nanofibrous mat cross-linked under identical experimental conditions (0.25% GA, 20 min) was used as a control. The log and bacterial inhibition (%) values for the PVSA/AMOX nanofibrous mat at different time intervals are depicted in Table 4 and Fig. 4, respectively. The results demonstrated that PVSA/AMOX nanofibrous mats showed antibacterial efficacy on test bacteria. After 4 h, 1.78 log and 1.03 log reduction were determined on *S. aureus* and *E. coli*, respectively. The log reduction was time-dependent for the test strains. The integration of the antibiotics into the nanofibers via the electrospinning method did not compromise its intrinsic antimicrobial properties, as described by Alavarse et al. [55], Schneider et al. [56], and Wang et al. [57]. Our results are similar to those previously described.

In each period applied in this study, *E. coli* was more resistant than *S. aureus* against amoxicillin, a result that correlates with the literature [58]. After 2 h, it was determined that the logarithmic decrease in the growth of *S. aureus* was statistically higher than that of *E. coli* ($p < 0.05$). The result might be

related to the differences in cell wall structure between Gram-negative and Gram-positive bacteria. It is well-known that Gram-negative bacteria generally show resistance against antimicrobial agents due to complex cell walls, including peptidoglycan complex-lipoprotein and outer membrane. On the other hand, the cell wall of Gram-positive bacteria comprises a peptidoglycan layer with lots of pores. Due to the porous cell wall of *S. aureus*, compounds easily permeate [43, 58].

As shown in Fig. 4, bacterial inhibition (%) values increased time-dependent on test bacteria. The inhibition percentage of *E. coli* at all tested times was lower than that of *S. aureus*. After 24 h, *S. aureus* and *E. coli* were inhibited at 44.87% and 30.25%, respectively.

Similar results were obtained with the disc diffusion method. While the inhibition zone of cross-linked PVSA/AMOX nanofibrous mats against *S. aureus* was recorded as 23.3 ± 0.6 mm, 11.0 ± 0.2 mm zone was determined for *E. coli* (Fig. 5). An inhibition zone was not observed for cross-linked PVSA (control) nanofibers.

3.4 Properties of the PVSA/AMOX Nanofibrous Mat

The mechanical, chemical, and physical characteristics of a wound dressing are essential factors in accelerating skin regeneration [59]. Therefore, the porosity, swelling, wettability, degradation, thickness, air permeability, tensile strength, and WVTR of the PVSA/AMOX nanofibrous mat cross-linked with 0.25% GA concentration for 20 min were investigated and evaluated in detail.

The porosity of the PVSA/AMOX nanofibrous mat was determined via BET and mercury porosimetry analyses since the pore size of a wound dressing is a determinative parameter for swelling, wettability, degradation, air permeability, WVTR, and wound healing properties. BET and mercury
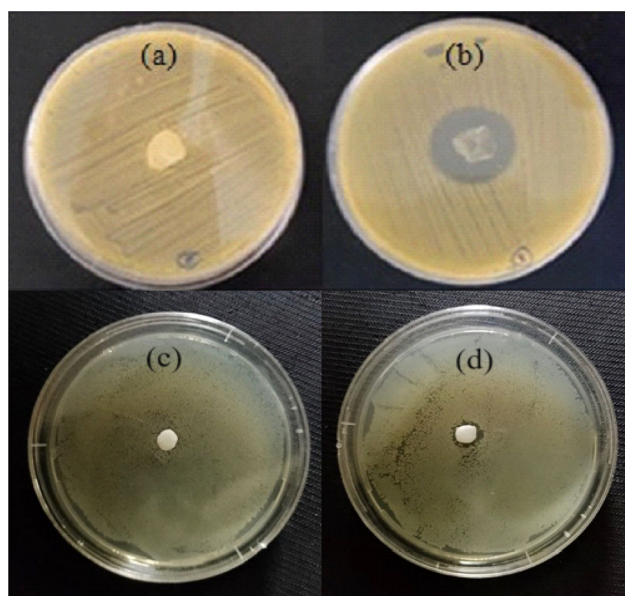
Fig. 5 Growth inhibition zones at the incubation time of 24 h: **a** *S. aureus*-the cross-linked PVSA (control); **b** *S. aureus*-the cross-linked PVSA/AMOX nanofibrous mats; **c** *E. coli*-the cross-linked PVSA (control); **d** *E. coli*-the cross-linked PVSA/AMOX nanofibrous mats

porosimetry analyses determine the pores in nano- and micro-size, respectively. The adsorption/desorption isotherms of nitrogen and pore size distribution are given in Figure SI4. The BET surface area of the PVSA/AMOX nanofibrous mat was 59.25 m^2/g, and the pore volume was 0.0534 cm^3/g. The pore size ranged between 1.89 and 16.87 nm, demonstrating that the PVSA/AMOX nanofibers have micropores and mesopores according to the IUPAC definition. The total porosity of the PVSA/AMOX nanofibrous mat was 59.4%, which is in the preferred range of 60–90% for cell adhesion, migration, and proliferation. Total interparticle porosity was 57.1%, and total intraparticle porosity was 2.3%. The pore sizes were distributed in the range of 1–7 μm, matching the human tissue cell sizes, which would benefit wound healing [60]. The pore size distribution graph is given in Figure SI5.

The swelling profile of a wound dressing is determinative in the absorption of excess exudate to provide a moist micro-environment in the wound area. In this way, the wound is protected from infections. Additionally, moisture is beneficial for wound healing and enables the unpainful removal of the wound dressing [61]. Due to their high surface area-to-volume ratio and hydrophilicity, nanofibrous mats absorb large amounts of exudate. The swelling kinetics of the PVSA and PVSA/AMOX nanofibrous mats are depicted in Figure SI6. The swelling ratio of both nanofibrous mats reached the equilibrium value after 10 min. The cross-linked PVSA nanofiber surface has a swelling ratio of 331 ± 13.1%, while the swelling ratio of PVSA/AMOX was 319 ± 4.2%. AMOX in the nanofibrous mat causes an insignificant change in the

swelling ratio. As a result, the PVSA/AMOX nanofibrous mat is suitable for use as a wound dressing with a high swelling ratio [62].

The WCA of a surface gives valuable information about the hydrophilicity of the material. A hydrophilic surface has lower contact angle values than 90º [63]. Hydrophilicity is one of the most critical factors affecting the intracellular compatibility of biomaterials. Cell adhesion and growth are directly affected by the wettability of the surfaces [64]. The WCAs of the cross-linked PVSA and PVSA/AMOX nanofibrous mats were measured, and the changes were determined at 1 s intervals. The obtained results are depicted in Figure SI7. The WCA of the cross-linked PVSA nanofibrous mat was 95.8° ± 1.8 in the first second. After 9 s, the WCA reached a value of less than 19.1 ± 1.2°, and the drop completely disappeared. On the other hand, the WCA of the cross-linked PVSA/AMOX nanofibrous mat was 73.4 ± 1.2° in the first second and reached a value of 29.9 ± 3.2° in the fourth second. The results show that the hydrophilicity and water absorbency of the PVSA/AMOX nanofibrous mat were higher than those of PVSA, probably because AMOX was loaded into the nanofibers. The hydrophilicity of PVSA/AMOX nanofibrous mat is an advantage in terms of absorption of wound exudate and rapid initiation of AMOX release against the risk of infection.

The degradability of a wound dressing plays a crucial role in potential biomedical applications. The controlled release of the therapeutic agent to the wounded area is possible via a biodegradable wound dressing [65]. However, partial degradability allows cell diffusion, nutrient flow, and integration of the wound dressing with host tissue [66]. The results of hydrolytic degradation studies showed that the degradation ratio of PVSA nanofibrous mat was 1.8 ± 0.2% at the end of 10 days. At the end of the same period, the degradation ratio was 2.2 ± 0.1% for the PVSA/AMOX nanofibrous mat (Figure SI8). The degradation rate of both surfaces reached the equilibrium value within 10 days. The type and severity of the wound can influence the choice of dressing degradation. Acute wounds with a predictable healing timeline may benefit from non-degradable dressings. On the other hand, for chronic wounds or situations where the dressing needs to remain in contact with the wound for an extended period, a degradable dressing may be more appropriate. The results show that the cross-linked PVSA/AMOX nanofiber surface is highly resistant to hydrolytic degradation.

The mechanical properties of a wound dressing are essential in terms of the motorial behavior of the skin [67]. A suitable wound dressing material should be strong and flexible to control external stress on the skin [68]. While the elongation and tensile strength of human skin range from 35–115% to 5–30 MPa, respectively [69], a standard medical material should meet values of the elongation between 17 and 207% and tensile strength between 1 and 24 MPa [70].

The PVSA/AMOX nanofibrous mat showed good mechanical properties within the ranges of human skin's values, with a tensile strength of 6.73 ± 0.48 MPa and elongation at a maximum load of $81.9 \pm 17.0\%$. The load-elongation graph is given in Figure SI9. The strength and elongation values of PVSA nanofibrous mats were reported as 1.23 MPa and 13.8% [70], 6.76 MPa and 11.3% [25], 10.66 MPa and 15.9% [71] and 20.5 MPa and 150% [72], respectively. Considering that the mechanical properties of nanofibrous mats depend on various factors such as composition, structure, and interaction between nanofibers and nanofiber diameter [25, 73], it was not expected to be similar to previous literature.

Oxygen, which causes the re-epithelialization, angiogenesis, collagen synthesis, oxidative killing of bacteria, and thus faster healing, is vital in wound healing [74]. The air permeability of a wound dressing allows oxygen to enter and make contact with the wound [75]. However, excessive air permeability may adversely affect the healing process, causing the wound to dry and turning the wound dressing into a nonocclusive material [75, 76]. Many structural parameters can affect the air permeability of the nanofibrous membranes, such as fiber diameter, morphology, thickness, density, wettability, pore size, and porosity of the membrane [76, 77]. The finer the fibers, the smaller the pores, and generally, if tiny pores increase within the same area, air permeability will decrease. Due to the rise of friction and pressure loss, air passage from the pores is difficult when the membrane thickness increases [76–78]. The thickness of the cross-linked PVSA/AMOX nanofibrous mat was determined as 0.43 ± 0.08 mm, which is suitable for use as a wound dressing [79]. The air permeability was also 17.2 ± 4.91 L/m^2/s. The air permeability values of calcium alginate-based nonwoven commercial wound dressing and commercial cotton gauze were 787.4 L/m^2/s [76] and 470.13 L/m^2/s [80], respectively. This high difference was thought to be due to the high density of nanofibrous mats. On the other hand, the air permeability values of nanofibrous mats given in the literature were also complicated because of their lightness and thinness [81].

A high value of WVTR could be a reason for wound dehydration and scar production, while a low WVTR value may not provide enough moisture for wound healing. The WVTR of Op Site (Smith & Nephew), Duoderm (ConvaTec Ltd), Metoderm (ConvaTec Ltd), and Biobrain® commercial wound dressing is 792 ± 32, 886 ± 60, 823 ± 45, and 1565 ± 51 g/m^2/d, respectively [82]. The PVSA/AMOX nanofibrous mat with a WVTR of 1485 ± 13.6 g/m^2/d was suitable as a wound dressing.
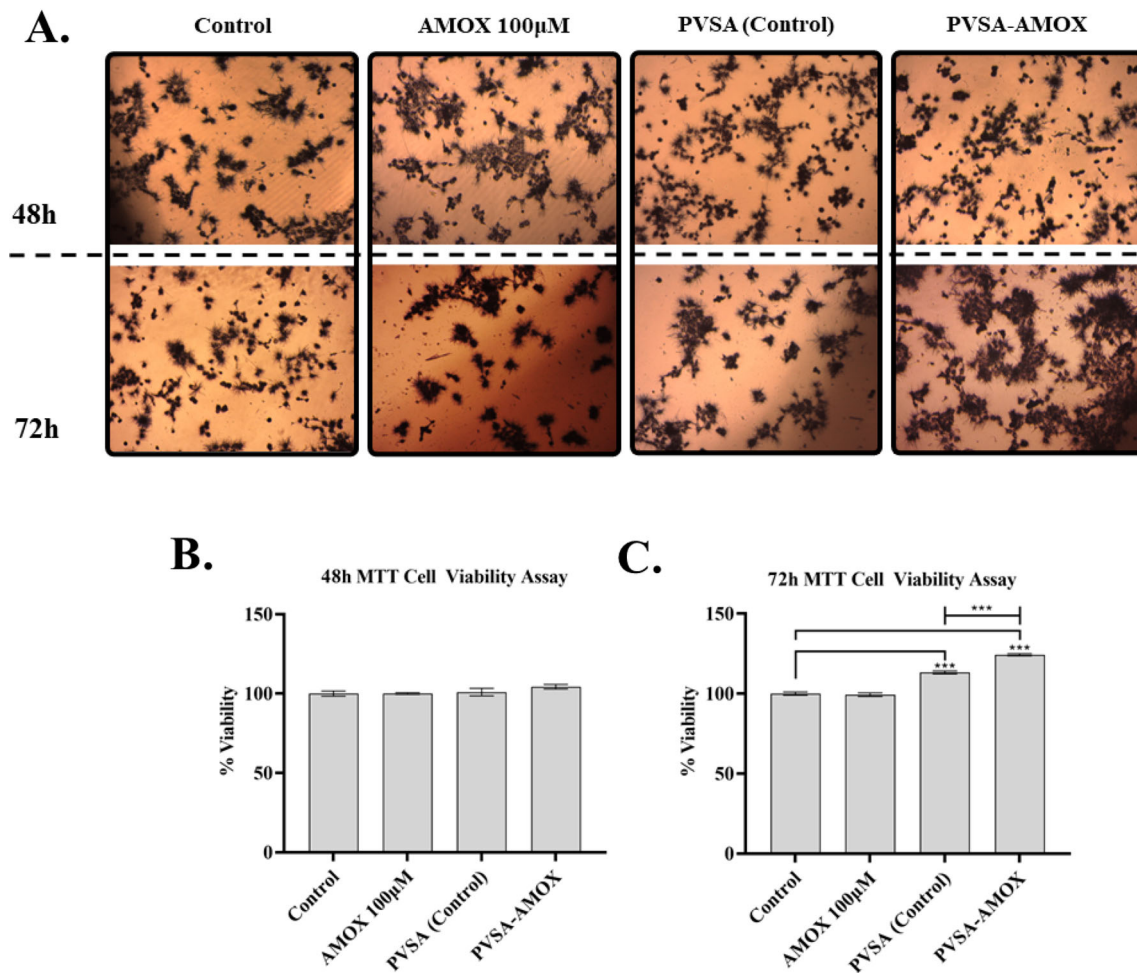
3.5 Cytotoxicity

The skin is the first barrier in the human body against external influences such as external mechanical forces, chemical compounds, UV, and pathogens. Skin damage against external influences undergoes a complex tissue regeneration process involving hemostasis, inflammation, proliferation, and remodeling [83, 84]. Therefore, the nanofiber mats are expected to be non-cytotoxic and biocompatible and promote the fundamental processes in the wound healing mechanism [85]. For this purpose, the cytotoxic effect profile of PVSA/AMOX nanofibrous mats was determined using MTT cell viability assay. Since PVSA/AMOX nanofibrous mats contain AMOX equal to 100 µM concentration in the studied volume, 100 µM AMOX was also used as a control. After 48 h of incubation, PVSA and PVSA/AMOX nanofibrous mats showed no cytotoxic effect on HaCaT cell lines (Fig. 6B). In microscopic examinations, no changes were observed in cell density compared to the control. In addition, stable formazan crystal formations may indicate that the cells are metabolically active (Fig. 6A). After 72 h of incubation, 113% cell viability was observed in the PVSA sample group and 124% in the PVSA/AMOX group (Fig. 6C). The increase in cell proliferation may indicate that the biocompatibility of nanofibrous mats is quite high. The microstructure of nanofibers prepared by electrospinning technology is very important in their compatibility with the extracellular matrix. Promoting electrospinning technology with combinations of bioactive scaffolds such as SA and synthetic structures such as PVA can show excellent properties in wound healing [2, 86, 87]. At the end of the 72-h incubation period, the increase in cell proliferation indicates that the PVSA nanofibrous mats produced support cell proliferation by mimicking the ECM matrix.

4 Conclusion

In this study, an amoxicillin-loaded polyvinyl alcohol/sodium alginate nanofibrous mat was developed via electrospinning, and its drug release properties, antibacterial activity, cytotoxicity, and physical performance were investigated. The nanofibrous mat was morphologically and chemically characterized, and the effect of cross-linker (GA) concentration and cross-linking time on the morphology and AMOX release profile were determined. The lower the GA concentration, the higher the number of fusions at junction points of the nanofibers. However, the cross-linking time did not drastically change the nanofiber morphology and the average nanofiber diameter. At a GA concentration of 0.25%, controlled AMOX release was observed with a cumulative release of 73.07% and 55.71% for 90 min at 20 and 40 min cross-linking time, respectively. The drug release mechanism obeyed the Korsmeyer-Peppas model with a release exponent smaller than 0.5. The properties of the PVSA/AMOX nanofibrous mat cross-linked with 0.25% GA solution for 20 min were characterized in detail, and it was used in antibacterial activity and cytotoxicity studies. The total porosity was

Fig. 6 Assessment of cytotoxicity profiles of nanofiber mats by MTT cell viability assay. **A** Formazan crystals formed by HaCaT cells in MTT cell viability assay. MTT cell viability assay; 48 h (**B**), 72 h (**C**).

*Denotes statically significant differences in comparison with control and PVSA: *($p < 0.05$), **($p < 0.01$) and ***($p < 0.001$). Data are presented as mean $\pm$ SD (n = 6)

59.4%, which is proper for cell adhesion, migration, and proliferation. The PVSA/AMOX nanofibrous mat has high swelling (319 $\pm$ 4.2%) and low degradation (2.2 $\pm$ 0.1% in 10 days) ratios. The WCA of the nanofibrous mat's surface was 73.4° $\pm$ 1.2, demonstrating the high hydrophilicity for exudate absorption. The nanofibrous mat has a tensile strength of 6.73 $\pm$ 0.48 MPa and elongation at a maximum load of 81.9 $\pm$ 17.0%, within the ranges of human skin's values. The thickness, air permeability, and WVTR of the PVSA/AMOX nanofibrous mat were 0.43 $\pm$ 0.08 mm, 17.2 $\pm$ 4.91 L/m^2/s and 1485 $\pm$ 13.6 g/m^2/d, respectively, which were suitable for wound dressing applications. The qualitative and quantitative studies proved that the PVSA/AMOX nanofibrous mat has antibacterial activity on *S. aureus* and *E. coli* bacteria. In addition, the nanofibrous mat has no cytotoxic effect on human normal keratinocyte cells. As a result, the AMOX-loaded nanofibrous mat has application potential in the biomedical area as a wound dressing. In vivo studies will be planned for future studies.

Author Contributions AÇ: Methodology, Investigation. ESD: Methodology, Investigation. EK: Validation, Supervision. ÇBG: Validation, Methodology. BO: Validation, Supervision, Conceptualization, Supervision.

Data Availability The supporting information file includes all data.

Declarations

Conflict of Interest The authors have no relevant financial or nonfinancial interests to disclose.

Ethical Approval Not applicable.

Consent for Publication All authors consented to this publication.

Consent to Participate Not applicable.

References

1. Saghazadeh, S.; Rinoldi, C.; Schot, M.; Kashaf, S.S.; Sharifi, F.; Jalilian, E.; Nuutila, K.; Giatsidis, G.; Mostafalu, P.; Derakhshandeh, H.; Yue, K.; Swieszkowski, W.; Memic, A.; Tamayol, A.; Khademhosseini, A.: Drug delivery systems and materials for wound healing applications. Adv. Drug Deliv. Rev. **127**, 138–166 (2018)

2. Boateng, J.; Catanzano, O.: Advanced therapeutic dressings for effective wound healing-a review. J. Pharm. Sci. **104**(11), 3653–3680 (2015)

3. Murphy, P.S.; Evans, G.R.: Advances in wound healing: a review of current wound healing products. Plast. Surg. Int. (2012). https://doi.org/10.1155/2012/190436

4. Kanani, A.G.; Bahrami, S.H.: Review on electrospun nanofibers scaffold and biomedical applications. Trends Biomater. Artif. Organs **24**(2), 93–115 (2010)

5. Azimi, B.; Maleki, H.; Zavagna, L.; De la Ossa, J.G.; Linari, S.; Lazzeri, A.; Danti, S.: Bio-based electrospun fibers for wound healing. J. Funct. Biomater. **11**(3), 67 (2020)

6. Kenawy, E.R.; Bowlin, G.L.; Mansfield, K.; Layman, J.; Simpson, D.G.; Sanders, E.H.; Wnek, G.E.: Release of tetracycline hydrochloride from electrospun poly(ethylene-*co*-vinylacetate), poly (lactic acid), and a blend. J. Control. Release **81**, 57–64 (2002)

7. Tra Thanh, N.; Ho Hieu, M.; Tran Minh Phuong, N.; Do Bui Thuan, T.; Nguyen Thi Thu, H.; Thai, V.P.; Do Minh, T.; Nguyen Dai, H.; Vo, V.T.; Nguyen Thi, H.: Optimization and characterization of electrospun polycaprolactone coated with gelatin-silver nanoparticles for wound healing application. Mater. Sci. Eng. C **91**, 318–329 (2018)

8. Lowe, A.; Bills, J.; Verma, R.; Lavery, L.; Davis, K.; Balkus, K.J.: Electrospun nitric oxide releasing bandage with enhanced wound healing. Acta Biomater. **13**, 121–130 (2015)

9. Spasova, M.; Manolova, N.; Paneva, D.; Mincheva, R.; Dubois, P.; Rashkov, I.; Maximova, V.; Danchev, D.: Polylactide stereocomplex-based electrospun materials possessing surface with antibacterial and hemostatic properties. Biomacromol **11**(1), 151–159 (2010)

10. Kataria, K.; Gupta, A.; Rath, G.; Mathur, R.B.; Dhakate, S.R.: In vivo wound healing performance of drug loaded electrospun composite nanofibers transdermal patch. Int. J. Pharm. **469**(1), 102–110 (2014)

11. Dwivedi, C.; Pandey, H.; Pandey, A.C.; Patil, S.; Ramteke, P.W.; Laux, P.; Luch, A.; Singh, A.V.: In vivo biocompatibility of electrospun biodegradable dual carrier (antibiotic + growth factor) in a mouse model-implications for rapid wound healing. Pharmaceutics **11**(4), 180 (2019)

12. Hassan, C.M.; Peppas, N.A.: Structure and applications of poly (vinyl alcohol) hydrogels produced by conventional crosslinking or by freezing/thawing methods. Biopolym.· PVA Hydrog. Anionic Polymerisation Nanocomposites, 37–65 (2000)

13. Barnett, S.; Varley, S.: The effects of calcium alginate on wound healing. Ann. R. Coll. Surg. Engl. **69**(4), 153 (1987)

14. Üstündağ, G.C.; Karaca, E.; Özbek, S.; Çavuşoğlu, İ: In vivo evaluation of electrospun poly (vinyl alcohol)/sodium alginate nanofibrous mat as wound dressing Tekst. Konfeksiyon **20**, 290–298 (2010)

15. Safi, S.; Morshed, M.; Hosseini Ravandi, S.A.; Ghiaci, M.: Study of electrospinning of sodium alginate, blended solutions of sodium alginate/poly(vinyl alcohol) and sodium alginate/poly(ethylene oxide). J. Appl. Polym. Sci. **104**, 3245–3255 (2007)

16. Rathna, G.V.N.; Birajdar, M.S.; Bhagwani, M.; Paul, V.L.: Studies on fabrication, characterization, and metal extraction using metal chelating nonwoven nanofiber mats of poly(vinyl alcohol) and sodium alginate blends. Polym. Eng. Sci. **53**, 321–333 (2013)

17. Islam, M.S.; Karim, M.R.: Fabrication and characterization of poly (vinyl alcohol)/alginate blend nanofibers by electrospinning method. Colloids Surf A Physicochem Eng Asp **366**(1–3), 135–140 (2010)

18. Saraiva, M.M.; Campelo, M.S.; Câmara Neto, J.F.; Lima, A.B.N.; Silva, G.A.; Dias, A.T.F.; Ricardo, N.M.P.S.; Kaplan, D.L.: Alginate/polyvinyl alcohol films for wound healing: advantages and challenges. J. Biomed. Mater. Res. **111**(1), 220–233 (2023)

19. Pakolpakçıl, A.; Osman, B.; Tümay Özer, E.; Sahan, Y.; Becerir, B.; Goktalay, G.; Karaca, E.: Halochromic composite nanofibrous mat for wound healing monitoring. Mater. Res. Express **6**, 1250 (2019)

20. Shalumon, K.T.; Anulekha, K.H.; Nair Sreeja, V.; Nair, S.V.; Chennazhi, K.P.; Jayakumar, R.: Sodium alginate/poly(vinyl alcohol)/nano ZnO composite nanofibers for antibacterial wound dressings. Int. J. Biol. Macromol. **49**(3), 247–254 (2011)

21. Li, W.; Li, X.; Chen, Y.; Li, X.; Deng, H.; Wang, T.; Huang, R.; Fan, G.: Poly(vinyl alcohol)/sodium alginate/layered silicate based nanofibrous mats for bacterial inhibition. Carbohydr. Polym. **92**(2), 2232–2238 (2013)

22. Rafiq, M.; Hussain, T.; Abid, S.; Nazir, A.; Masood, R.: Development of sodium alginate/PVA antibacterial nanofibers by the incorporation of essential oils. Mater. Res. Express **5**(3), 035007 (2018)

23. Fu, R.; Li, C.; Yu, C.; Xie, H.; Shi, S.; Li, Z.; Wang, Q.; Lu, L.: A novel electrospun membrane based on moxifloxacin hydrochloride/poly(vinyl alcohol)/sodium alginate for antibacterial wound dressings in practical application. Drug Deliv. **23**(3), 828–839 (2016)

24. Esentürk, İ; Balkan, T.; Güngör, S.; Saraç, A.S.; Erdal, M.S.: Preparation and characterization of naftifine-loaded poly(vinyl alcohol)/sodium alginate electrospun nanofibers. Braz. J. Pharm. Sci. **56**, 1–12 (2021)

25. Rezaei, M.; Nikkhah, M.; Mohammadi, S.; Bahrami, S.H.; Sadeghizadeh, M.: Nano-curcumin/graphene platelets loaded on sodium alginate/polyvinyl alcohol fibers as potential wound dressing. J. Appl. Polym. Sci. **138**(35), 50884 (2021)

26. Han, X.; Huo, P.; Ding, Z.; Kumar, P.; Liu, B.: Preparation of lutein-loaded PVA/sodium alginate nanofibers and investigation of its release behavior. Pharmaceutics **11**(9), 449 (2019)

27. Arthanari, S.; Mani, G.; Jang, J.H.; Choi, J.O.; Cho, Y.H.; Lee, J.H.; Cha, S.E.; Oh, H.S.; Kwon, D.H.; Jang, H.T.: Preparation and characterization of gatifloxacin-loaded alginate/poly (vinyl alcohol) electrospun nanofibers. Artif. Cells Nanomed. Biotechnol. **44**(3), 847–852 (2016)

28. Najafi, S.; Gholipour-Kanani, A.; Eslahi, N.; Hajir Bahrami, S.: Study on release of cardamom extract as an antibacterial agent from electrospun scaffold based on sodium alginate. J. Text. Inst. **112**(9), 1482–1490 (2021)

29. Castillo-Ortega, M.M.; Nájera-Luna, A.; Rodríguez-Félix, D.E.; Encinas, J.C.; Rodríguez-Félix, F.; Romero, J.; Herrera-Franco, P.J.: Preparation, characterization and release of amoxicillin from cellulose acetate and poly(vinyl alcohol) electrospun fibrous membranes. Mater. Sci. Eng. C **31**(8), 1772–1778 (2011)

30. Castillo-Ortega, M.M.; Montaño-Figueroa, A.G.; Rodríguez-Félix, D.E.; Munive, G.T.; Herrera-Franco, P.J.: Amoxicillin embedded in cellulose acetate-poly (vinyl pyrrolidone) fibers prepared by coaxial electrospinning: preparation and characterization. Mater. Lett. **76**, 250–254 (2012)

31. Kiatyongchai, T.; Wongsasulak, S.; Yoovidhya, T.: Coaxial electrospinning and release characteristics of cellulose acetate–gelatin blend encapsulating: a model drug. J. Appl. Polym. Sci. **131**(8), 40167 (2014)

32. Vashisth, P.; Srivastava, A.K.; Nagar, H.; Raghuwanshi, N.; Sharan, S.; Nikhil, K.; Pruthi, P.A.; Singh, R.P.; Roy, P.; Pruthi, V.: Drug functionalized microbial polysaccharide based nanofibers as transdermal substitute. Nanomed. NBM **12**(5), 1375–1385 (2016)

33. Gupta, P.; Purwar, R.: Electrospun pH responsive poly (acrylic acid-co- acrylamide) hydrogel nanofibrous mats for drug delivery. J. Polym. Res. **27**(10), 296 (2020)

34. Tang, Y.; Chen, L.; Zhao, K.; Wu, Z.; Wang, Y.; Tan, Q.: Fabrication of PLGA/HA (core)-collagen/amoxicillin (shell) nanofiber membranes through coaxial electrospinning for guided tissue regeneration. Compos. Sci. Technol. **125**, 100–107 (2016)

35. Chen, D.W.; Lee, F.Y.; Liao, J.Y.; Liu, S.J.; Hsiao, C.Y.; Chen, J.K.: Preclinical experiments on the release behavior of biodegradable nanofibrous multipharmaceutical membranes in a model of four-wall ıntrabony defect. Antimicrob. Agents Chemother. **57**(1), 9–14 (2013)

36. Yu, K.; Zhu, T.; Wu, Y.; Zhou, X.; Yang, X.; Wang, J.; Fang, J.; El-Hamshary, H.; Al-Deyab, S.S.; Mo, X.: Incorporation of amoxicillin-loaded organic montmorillonite into poly(ester-urethane) urea nanofibers as a functional tissue engineering scaffold. Colloids Surf. B **151**, 314–323 (2017)

37. Sofokleous, P.; Stride, E.; Edirisinghe, M.: Preparation, characterization, and release of amoxicillin from electrospun fibrous wound dressing patches. Pharm. Res. **30**(7), 1926–1938 (2013)

38. Ojah, N.; Borah, R.; Ahmed, G.A.; Mandal, M.; Choudhury, A.J.: Surface modification of electrospun silk/AMOX/PVA nanofibers by dielectric barrier discharge plasma: physiochemical properties, drug delivery and in vitro biocompatibility. Prog. Biomater. **9**(4), 219–237 (2020)

39. Li, Q.; Guan, L.; Hong, W.; Liu, J.; Xing, G.: Preparation and research of electrospinning chitosan nanofiber sustained-release carrier. Integr. Ferroelectr. **144**(1), 48–55 (2013)

40. Li, X.; Wang, C.; Yang, S.; Liu, P.; Zhang, B.: Electrospun PCL/mupirocin and chitosan/lidocaine hydrochloride multifunctional double layer nanofibrous scaffolds for wound dressing applications. Int. J. Nanomed. **13**, 5287–5299 (2018)

41. Tamahkar, E.: Bacterial cellulose/poly vinyl alcohol based wound dressings with sustained antibiotic delivery. Chem. Pap. **75**, 3979–3987 (2021)

42. Wittaya, A.S.; Prahsarn, C.: Development and in vitro evaluation of chitosan-polysaccharides composite wound dressings. Int. J. Pharm. **313**(1–2), 123–128 (2006)

43. Ozcan, İ; Saricaoglu, F.T.; Parlak, M.E.; Dagdelen, A.F.; Yigit Cinar, A.; Gul, L.B.; Dundar, A.N.; Tosun, F.: Characterization of solution blow spun poly(lactic) acid based nanofibers containing sucuk spice mix essential oils. J. Polym. Environ. **31**, 2334–2346 (2023)

44. Liu, Q.; Ouyang, W.-C.; Zhou, X.-H.; Jin, T.; Wu, Z.-W.: Antibacterial activity and drug loading of moxifloxacin-loaded poly(vinyl alcohol)/chitosan electrospun nanofibers. Front. Mater. **8**, 643428 (2021)

45. Mosmann, T.: Rapid colorimetric assay for cellular growth and survival: application to proliferation and cytotoxicity assays. J. Immunol. Methods **65**(1–2), 55–63 (1983)

46. Ekambaram, R.; Dharmalingam, S.: Fabrication and evaluation of electrospun biomimetic sulphonated PEEK nanofibrous scaffold for human skin cell proliferation and wound regeneration potential. Mater. Sci. Eng. C **115**, 111150 (2020)

47. Zhao, Z.; Li, Y.; Wu, J.; Shi, Z.; Zhao, P.; Su, H.; Wang, Q.; Jin, L.: Nanofiber orodispersible films based on carboxymethyl curdlan and PEO: new delivery system for amlodipine besylate. Colloids Surf A Physicochem Eng Asp **635**, 128096 (2022)

48. Pakolpakçıl, A.; Osman, B.; Göktalay, G.; Özer, E.T.; Sahan, Y.; Becerir, B.; Karaca, E.: Design and in vivo evaluation of alginate-based ph-sensing electrospun wound dressing containing anthocyanins. J. Polym. Res. **28**, 50 (2021)

49. Altuntuğ Cesur, M.İ; Osman, B.; Özer, E.T.; Kanmaz, D.; Baykara, M.; Karaca, E.: Preparation and characterization of latanoprost-loaded PVA nanofibers as an ocular drug delivery system for glaucoma treatment. Int. J. Polym. Mater. Polym. Biomater. **73**(9), 761–770 (2024)

50. Shi, S.; Zhang, Z.; Luo, Z.; Yu, J.; Liang, R.; Li, X.; Chen, H.: Chitosan grafted methoxy poly(ethylene glycol)-poly(ε-caprolactone) nanosuspension for ocular delivery of hydrophobic diclofenac. Sci. Rep. **5**, 11337 (2015)

51. Bal, A.; Özkahraman, B.; Özbaş, Z.: Preparation and characterization of pH responsive poly(methacrylic acid-acrylamide-n-hydroxyethyl acrylamide) hydrogels for drug delivery systems. J. Appl. Polym. Sci. **133**, 43226 (2015)

52. Paarakh, M.P.; Jose, P.A.; Setty, C.M.; Christoper, G.P.: Release kinetics–concepts and applications. IJPRT **8**(1), 12–20 (2018)

53. Lowy, F.D.: *Staphylococcus aureus* infections. N. Engl. J. Med. **339**, 520e32 (1998)

54. Allocati, N.; Masulli, M.; Alexeyev, M.F.; Di Ilio, C.: *Escherichia coli* in Europe: an overview. Int. J. Environ. Res. Public Health **10**, 6235–6254 (2013)

55. Alavarse, A.C.; de Oliveira Silva, F.W.; Colque, J.T.; da Silva, V.M.; Prieto, T.; Venancio, E.C.; Bonvent, J.-J.: Tetracycline hydrochloride-loaded electrospun nanofibers mats based on PVA and chitosan for wound dressing. Mater. Sci. Eng. C **77**, 271–281 (2017)

56. Schneider, R.; Mercante, L.A.; Andre, R.S.; Brandão, H.D.M.; Mattoso, L.H.; Correa, D.S.: Biocompatible electrospun nanofibers containing cloxacillin: antibacterial activity and effect of pH on the release profile. React. Funct. Polym. **132**, 26–35 (2018)

57. Wang, S.; Zheng, F.; Huang, Y.; Fang, Y.; Shen, M.; Zhu, M.; Shi, X.: Encapsulation of amoxicillin within laponite-doped poly (lactic-*co*-glycolic acid) nanofibers: preparation, characterization, and antibacterial activity. ACS Appl. Mater. Interfaces **4**, 6393–6401 (2012)

58. Davis, C.A.; Janssen, E.M.: Environmental fate processes of antimicrobial peptides daptomycin, bacitracins, and polymyxins. Environ. Int. **134**, 105271 (2020)

59. Zhang, J.; Zheng, T.; Alarçin, E.; Byambaa, B.; Guan, X.; Ding, J.; Zhang, Y.S.; Li, Z.: Porous electrospun fibers with self-sealing functionality: An enabling strategy for trapping biomacro-molecules. Small **13**(47), 1701949 (2017)

60. Liu, Y.Q.; Feng, J.W.; Zhang, C.C.; Teng, Y.; Liu, Z.; He, J.H.: Air permeability of nanofiber membrane with hierarchical structure. Therm. Sci. **22**, 1637–1643 (2018)

61. Jiang, S.; Ma, B.C.; Huang, W.; Kaltbeitzel, A.; Kizisavas, G.; Crespy, D.; Zhang, K.; Landfester, K.: Visible light active nanofibrous membrane for antibacterial wound dressing. Nanoscale Horiz. **3**(4), 439–446 (2018)

62. Morgado, P.I.; Aguiar-Ricardo, A.; Correia, I.J.: Asymmetric membranes as ideal wound dressings: an overview on production methods, structure, properties and performance relationship. J. Membr. Sci. **490**, 139–151 (2015)

63. Li, C.; Zhang, J.; Han, J.; Yao, B.: A numerical solution to the effects of surface roughness on water–coal contact angle. Sci. Rep. **11**, 459 (2021)

64. Al-Azzam, N.; Alazzam, A.: Micropatterning of cells via adjusting surface wettability using plasma treatment and graphene oxide deposition. PLoS ONE **17**(6), e0269914 (2022)

65. Su, S.; Kang, P.M.: Systemic review of biodegradable nanomaterials in nanomedicine. Nanomaterials **10**(4), 656 (2020)

66. Capanema, N.; Mansur, A.; de Jesus, A.C.; Carvalho, S.M.; de Oliveira, L.C.; Mansur, H.S.: Superabsorbent cross-linked carboxymethyl cellulose-PEG hydrogels for potential wound dressing applications. Int. J. Biol. Macromol. **106**, 1218–1234 (2018)

67. Tan, L.; Hu, J.; Huang, H.; Han, J.; Hu, H.: Study of multifunctional electrospun composite electrospun mats for smart wound healing. Int. J. Biol. Macromol. **79**, 469–476 (2015)

68. Lin, Y.; Zhang, Y.; Cai, X.; He, H.; Yang, C.; Ban, J.; Guo, B.: Design and self-assembly of peptide-copolymer conjugates into nanoparticle hydrogel for wound healing in diabetes. Int. J. Nanomed. **19**, 2487–2506 (2024)

69. Narayanan, K.B.; Park, G.T.; Han, S.S.: Electrospun poly(vinyl alcohol)/reduced graphene oxide nanofibrous scaffolds for skin tissue engineering. Colloids Surf. B **191**, 110994 (2020)

70. Aloma, K.K.; Sukaryo, S.; Fahlawati, N.I.; Dahlan, K.; Oemar, S.: Synthesis of nanofibers from alginate-polyvinyl alcohol using electrospinning methods. Macromol. Symp. **391**(1), 1900199 (2020)

71. Sadeghi-Aghbash, M.; Rahimnejad, M.; Adeli, H.; Feizi, F.: Fabrication and development of PVA/alginate nanofibrous mats containing arnebia euchroma extract as a burn wound dressing. React. Funct. Polym. **181**, 105440 (2022)

72. Rafienia, M.; Saberi, A.; Poorazizi, E.: A novel fabrication of PVA/alginate-bioglass electrospun for biomedical engineering application. Nanomed. J. **4**(3), 152–163 (2017)

73. Sharma, A.; Gupta, A.; Rath, G.; Goyal, A.; Mathur, R.B.; Dhakate, S.R.: Electrospun composite nanofiber-based transmucosal patch for anti-diabetic drug delivery. J. Mater. Chem. B **1**(27), 3410–3418 (2013)

74. Yip, W.L.: Influence of oxygen on wound healing. Int. Wound J. **12**(6), 620–624 (2015)

75. Yang, Y.; Hu, H.: Spacer fabric-based exuding wound dressing—part II: comparison with commercial wound dressings. Text. Res. J. **87**, 481–1493 (2017)

76. Maver, T.; Hribernik, S.; Mohan, T.; Smrke, D.M.; Maver, U.; Stana-Kleinschek, K.: Functional wound dressing materials with highly tunable drug release properties. RSC Adv. **5**, 77873–77884 (2015)

77. Lee, K.; Lee, S.: Electrospun nanofibrous membranes with essential oils for wound dressing applications. Fibers Polym. **21**(5), 999–1012 (2020)

78. Mavruz, S.; Ogulata, R.T.: Investigation and statistical prediction of air permeability of cotton knitted fabrics. Tekstil ve Konfeksiyon **19**(1), 29–38 (2009)

79. Üstündağ Okur, N.; Hökenek, N.; Okur, M.E.; Ayla, Ş; Yoltaş, A.; Siafaka, P.I.; Cevher, E.: An alternative approach to wound healing field; new composite films from natural polymers for mupirocin dermal delivery. SPJ **27**(5), 738–752 (2019)

80. Liu, X.; Lin, T.; Fang, J.; Yao, G.; Zhao, H.; Dodson, M.; Wang, X.: In vivo wound healing and antibacterial performances of electrospun nanofibre membranes. J. Biomed. Mater. Res. A **94**, 499–508 (2010)

81. Afshari, M.: Electrospun nanofibers, 1st edn. Woodhead Publishing, Cambridge (2016)

82. Gharibi, R.; Yeganeh, H.; Abdali, Z.: Preparation of antimicrobial wound dressings via thiol–ene photopolymerization reaction. J. Mater. Sci. **53**(3), 1581–1595 (2018)

83. Maintz, L.; Bieber, T.; Simpson, H.D.; Demessant-Flavigny, A.L.: From skin barrier dysfunction to systemic impact of atopic dermatitis: implications for a precision approach in dermocosmetics and medicine. J. Pers. Med. **12**(6), 893 (2022)

84. El Ayadi, A.; Jay, J.W.; Prasai, A.: Current approaches targeting the wound healing phases to attenuate fibrosis and scarring. Int. J. Mol. Sci. **21**(3), 1105 (2020)

85. Liu, Y.; Li, C.; Feng, Z.; Han, B.; Yu, D.G.; Wang, K.: Advances in the preparation of nanofiber dressings by electrospinning for promoting diabetic wound healing. Biomolecules **12**(12), 1727 (2022)

86. Jadbabaei, S.; Kolahdoozan, M.; Naeimi, F.; Ebadi-Dehaghani, H.: Preparation and characterization of sodium alginate-PVA polymeric scaffolds by electrospinning method for skin tissue engineering applications. RSC Adv. **11**(49), 30674–30688 (2021)

87. Lv, H.; Zhao, M.; Li, Y.; Li, K.; Chen, S.; Zhao, W.; Wu, S.; Han, Y.: Electrospun chitosan-polyvinyl alcohol nanofiber dressings loaded with bioactive ursolic acid promoting diabetic wound healing. Nanomaterials **12**(17), 2933 (2022)